Hindawi Publishing Corporation
International Journal of Photoenergy
Volume 2016, Article ID 3095758, 7 pages
http://dx.doi.org/10.1155/2016/3095758

*Research Article*

# Study of Transition Region of p-Type $SiO_x$:H as Window Layer in a-Si:H/a-$Si_{1-y}Ge_y$:H Multijunction Solar Cells

**Pei-Ling Chen, Po-Wei Chen, and Chuang-Chuang Tsai**

*Department of Photonics, National Chiao Tung University, 1001 University Road, Hsinchu 300, Taiwan*

Correspondence should be addressed to Pei-Ling Chen; daphnechen0822orama@gmail.com

Received 27 May 2016; Revised 3 July 2016; Accepted 10 July 2016

Academic Editor: Yi Zhang



We have studied the p-type hydrogenated silicon oxide ($SiO_x$:H) films prepared in the amorphous-to-microcrystalline transition region as a window layer in a-Si:H/a-$Si_{1-y}Ge_y$:H multijunction solar cells. By increasing the $H_2$-to-$SiH_4$ flow ratio ($R_{H_2}$) from 10 to 167, the $SiO_x$:H(p) films remained amorphous and exhibited an increased hydrogen content from 10.2% to 12.2%. Compared to the amorphous $SiO_x$:H(p) film prepared at low $R_{H_2}$, the $SiO_x$:H(p) film deposited at $R_{H_2}$ of 167 exhibited a higher bandgap of 2.04 eV and a higher conductivity of $1.15 \times 10^{-5}$ S/cm. With the employment of $SiO_x$:H(p) films prepared by increasing $R_{H_2}$ from 10 to 167 in a-Si:H single-junction cell, the FF improved from 65% to 70% and the efficiency increased from 7.4% to 8.7%, owing to the enhanced optoelectrical properties of $SiO_x$:H(p) and the improved p/i interface. However, the cell that employed $SiO_x$:H(p) film with $R_{H_2}$ over 175 degraded the p/i interface and degraded the cell performance, which were arising from the onset of crystallization in the window layer. Compared to the cell using standard a-$SiC_x$:H(p), the a-Si:H/a-$Si_{1-y}Ge_y$:H tandem cells employing $SiO_x$:H(p) deposited with $R_{H_2}$ of 167 showed an improved efficiency from 9.3% to 10.3%, with $V_{OC}$ of 1.60 V, $J_{SC}$ of 9.3 mA/cm$^2$, and FF of 68.9%.

## 1. Introduction

Silicon-based thin-film solar cells have the advantages of low material usage, low temperature process, and capability of using flexible substrate, which can be produced for large-scale and low-cost applications [1, 2]. The conversion efficiency of silicon-based thin-film solar cells is relatively lower which needs to be further improved. One of the approaches in terms of obtaining high efficiency is the development of multijunction solar cells for more efficient utilization of solar spectrum [3, 4]. It has been shown that the hydrogenated amorphous silicon germanium (a-$Si_{1-y}Ge_y$:H) is a promising material as low-bandgap absorber in multijunction solar cells, due to its higher absorption coefficient compared to the hydrogenated amorphous silicon (a-Si:H) [5]. Studies have also reported that the a-Si:H/a-$Si_{1-y}Ge_y$:H tandem cell offered a high efficiency with broadband absorption, low absorber thickness, and high production throughput, which has attracted much attention to be employed in the triple- or multijunction solar cells [6, 7].

To further achieve high efficiency of a-Si:H/a-$Si_{1-y}Ge_y$:H solar cells, the employment of an ideal window layer is required. The window layer can affect both light absorption and carrier transport in the solar cells [8, 9]. The p-type hydrogenated amorphous silicon carbide (a-$SiC_x$:H(p)) has been widely used as window layer in amorphous silicon-based solar cells due to its wide bandgap [10]. However, alloying carbon induced defects in the a-Si:H network, which hindered the carrier collection in solar cells [11]. The p-type hydrogenated amorphous silicon oxide (a-$SiO_x$:H(p)) has been reported as an alternative to a-$SiC_x$:H(p) due to its better electrical property, which was attributed to the less defects density in a-$SiO_x$:H(p) [12].

To improve the quality of a-$SiO_x$:H(p), an appropriate hydrogen dilution was needed during the deposition. The hydrogen radicals during film growth enhanced the passivation of dangling bonds on the growing surface and promoted the structural relaxation of the silicon network [13, 14]. On the other hand, abundant hydrogen radicals may also lead to phase transition from amorphous to microcrystalline

structures, which decreased the bandgap of p-layer and increased the band offset at p/i interface [15]. It has been reported that the undoped or p-type a-Si:H prepared in the transition region resulted in a lower defect density at the p/i interface and thus reduced the recombination velocity [16]. Moreover, it has also been pointed out that the undoped $SiO_x$:H in the transition region exhibited higher bandgap of 1.88 eV, accompanied with an increased photosensitivity over 2 orders of magnitude by increasing hydrogen gas flow [15]. However, only few researches studied and focused on the structural and optoelectrical properties of p-type $SiO_x$:H prepared in the amorphous-to-microcrystalline transition region, as well as the corresponding cell performance.

In this work, we have developed the p-type $SiO_x$:H from amorphous phase to microcrystalline phase by optimizing the deposition conditions including $H_2$-to-$SiH_4$ flow ratio ($R_{H_2}$). The effects of $R_{H_2}$ on structural analysis, chemical composition, and optoelectrical properties of $SiO_x$:H(p) films were systematically studied. Furthermore, the effect of $SiO_x$:H(p) films deposited at different $R_{H_2}$ as window layer in a-Si:H single-junction cells was analyzed in detail. The characteristics of the optimized $SiO_x$:H(p) substituted for the conventional a-$SiC_x$:H(p) as window layer in a-Si:H/a-$Si_{1-y}Ge_y$:H tandem solar cells, which were designed for multijunction solar cells, were also presented.

## 2. Experimental Details

Silicon-based thin films were prepared in a 27.12 MHz single-chamber plasma-enhanced chemical vapor deposition (PECVD) system with a load-lock transfer chamber. Gas mixtures of $SiH_4$, $CO_2$, $GeH_4$, $B_2H_6$, $PH_3$, and $H_2$ were used as source gases. The p-type $SiO_x$:H films were prepared at different $R_{H_2}$ on Corning EAGLE XG glass substrate at approximately 190°C. The oxygen content ([O]) of $SiO_x$:H(p) films was examined by X-ray photoelectron spectroscopy (XPS). The hydrogen content ($C_H$) of $SiO_x$:H(p) films was calculated by the integrated strength of the rocking-wagging-rolling vibration at 640 $cm^{-1}$, which was characterized by Fourier transform infrared spectroscopy (FTIR). The transmittance and reflectance of films were measured by an ultraviolet-visible near-infrared spectrophotometer for calculating the absorption coefficient. The value of bandgap ($E_g$) of a-$SiO_x$:H(p) was determined by using Tauc's formula [17]. The Raman spectrum of $SiO_x$:H(p) was deconvoluted to four Gaussian peaks centered at 430, 480, 510, and 520 $cm^{-1}$, which corresponded to the longitudinal optical (LO) mode of a-Si:H, the transverse optical (TO) mode of a-Si:H, the intermediate fraction mode of c-Si, and the TO mode of c-Si, respectively [18]. The crystalline volume fraction ($X_C$) of $\mu$c-$SiO_x$:H(p) was calculated from the ratio of the integrated intensities of deconvoluted TO mode peaks centered at 480, 510, and 520 $cm^{-1}$ from Raman spectroscopy with a probe laser of 488 nm excitation. The dark conductivity ($\sigma_d$) of $SiO_x$:H(p) films was measured with coplanar Ag electrodes at room temperature. The activation energy ($E_a$) of $SiO_x$:H(p) films was calculated from temperature dependence of dark conductivity using the Arrhenius Plot.

The a-Si:H single-junction solar cells were deposited in a superstrate configuration on textured $SnO_2$:F glass substrate. The structure of a-Si:H single-junction solar cells was glass/$SnO_2$:F/$SiO_x$:H(p)/a-Si:H(i)/$\mu$c-$SiO_x$:H(n)/Ag with 12 nm thick $SiO_x$:H(p) window layer and 300 nm thick a-Si:H absorber. The thicknesses of the absorbers of a-Si:H/a-$Si_{1-y}Ge_y$:H tandem cells were 130 nm and 240 nm, respectively. The current density-voltage ($J$-$V$) characteristics of a-Si:H single-junction and a-Si:H/a-$Si_{1-y}Ge_y$:H tandem cells were obtained under a single lamp solar simulator with an Ag electrode area of 0.25 $cm^2$ defined by the shadow mask. The external quantum efficiency (EQE) was acquired under short-circuit condition, and the obtained short-circuit current density ($J_{SC}$) was used for the calculation of the cell performances.

## 3. Results and Discussion

*3.1. Structural, Optical, and Electrical Properties of p-Type $SiO_x$:H Thin Films.* The Raman spectra of $SiO_x$:H(p) as a function of $R_{H_2}$ are demonstrated in Figure 1. As $R_{H_2}$ increased from 10 to 167, the LO mode and the TO mode of a-Si:H were observed, which indicated that the film network was amorphous. Furthermore, the peak position of the TO mode of a-Si:H was shifted from 466 to 480 $cm^{-1}$ with increasing $R_{H_2}$ from 10 to 167. Studies have reported that the a-Si:H TO mode exhibiting a blue-shifted peak position correlated to the decreased bond angle distortion in the film network [19, 20]. It is pointed out that the decreased bond angle distortion can improve the stability of solar cell against light-induced degradation [21].

With increasing $R_{H_2}$ from 167 to 175, the intermediate fraction mode of c-Si around 510 $cm^{-1}$ was observed, suggesting the formation of microcrystalline structures. This led to the enhancement in the crystalline volume fraction ($X_C$) of $SiO_x$:H(p) from 0 to 25%. Further increasing $R_{H_2}$ from 175 to 300, the peak of the TO mode of c-Si appeared. This can be attributed to the fact that the excess hydrogen radicals enhanced the etching effect, which increased the relaxation of the disordered structures and the construction of Si-Si bond [22]. The increased $\mu$c-Si:H phase accompanied with the decreased a-Si:H phase further increased $X_C$ of $\mu$c-$SiO_x$:H(p) from 25 to 48%. In our case, the crystallite formation in the $SiO_x$:H(p) film in the amorphous-to-microcrystalline transition region was observed as $R_{H_2}$ was over 167.

In order to clarify the correlation between the structural change and the chemical composition of $SiO_x$:H(p) films, the oxygen and hydrogen contents were characterized. Figure 2(a) shows the oxygen content ([O]) of $SiO_x$:H(p) films as a function of $R_{H_2}$. As $R_{H_2}$ was increased from 10 to 300, [O] was slightly increased from 16 to 20 at. %. This was likely due to the hydrogen atoms assisting the dissociation of $CO_2$ into CO + OH, which resulted in the increased oxygen incorporation in film [23]. In addition, [O] of $SiO_x$:H(p) films was increased linearly from purely amorphous phase to microcrystalline phase. [O] seemed not to be affected by the formation of microcrystalline phase. This was due to

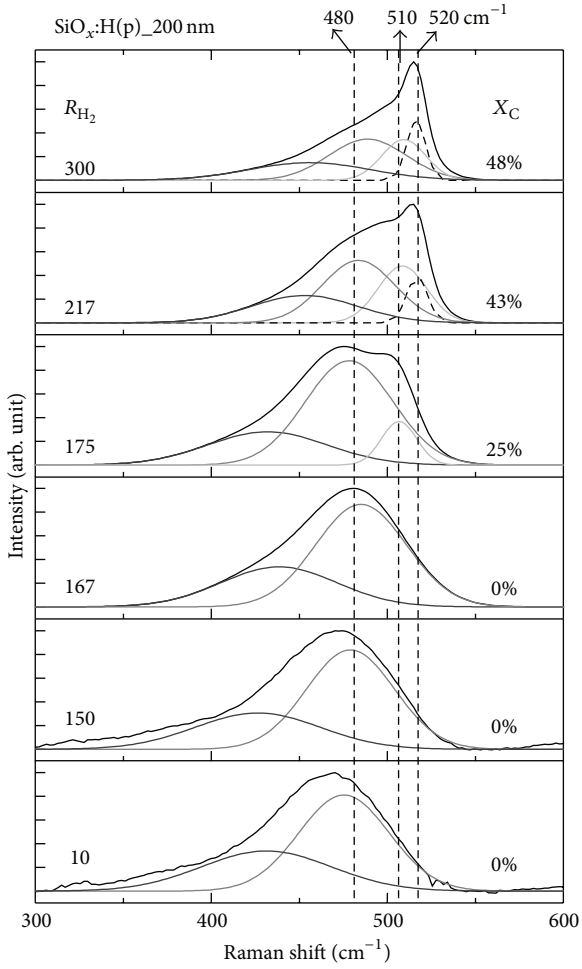


FIGURE 1: Raman spectrum and crystalline volume fraction for p-type SiO$_x$:H deposited at different $H_2$-to-$SiH_4$ flow ratio ($R_{H_2}$).

the mixed-phase nature of $\mu$c-SiO$_x$:H(p) films whose optical property was mainly affected by a-SiO$_x$:H phase where the oxygen was incorporated [24].

$C_H$ of SiO$_x$:H(p) films as a function of $R_{H_2}$ is shown in Figure 2(b). With increasing $R_{H_2}$ from 10 to 117, there is no significant change on $C_H$. This suggested that the network of a-SiO$_x$:H did not change obviously with increasing the hydrogen dilution. With increasing $R_{H_2}$ from 117 to 167, $C_H$ was increased from 10.2 to 12.2%. The increased $C_H$ seemed to correlate with the blue-shifted position of the TO mode of a-Si:H as shown in Figure 1. This suggested that small crystallites, which were not discerned by Raman spectroscopy, may exist in the network of SiO$_x$:H(p) [21]. The hydrogen passivated the dangling bonds around the crystallites where the structural defects may exist, leading to the improved network, less interface defects, and increased $C_H$ of SiO$_x$:H(p) film [25]. Further increasing $R_{H_2}$ from 167 to 300, $C_H$ was decreased from 12.2 to 5.4%. As illustrated in Figure 1, the microcrystalline phase was formed as $R_{H_2}$ was over 167. The decreased $C_H$ was thus likely due to the formation of ordered structure where the dangling bond was substantially reduced and thus less hydrogen was incorporated for passivation. In our case, we found that $R_{H_2}$ increased from 117 to 167, which was also before the onset of crystallization, which could increase $C_H$ of SiO$_x$:H(p) and improve the film quality of SiO$_x$:H(p).

Figure 3 shows the absorption coefficient of the SiO$_x$:H(p) as a function of $R_{H_2}$. The absorption coefficient of our standard a-SiC$_x$:H(p) film was shown as a reference. Compared to a-SiO$_x$:H(p) deposited at $R_{H_2}$ of 10, the a-SiC$_x$:H(p) deposited at the same $R_{H_2}$ exhibited lower absorption coefficient, which was due to the higher bandgap ($E_g$) of a-SiC$_x$:H(p) (2.03 eV) than that of a-SiO$_x$:H(p) (1.96 eV). As $R_{H_2}$ was increased from 10 to 167, the blue-shifted absorption coefficient of a-SiO$_x$:H(p) was due to the increased oxygen incorporation in a-SiO$_x$:H phase [26]. This increased $E_g$ from 1.96 to 2.04 eV. We also found that the $\mu$c-SiO$_x$:H(p) deposited at $R_{H_2}$ above 167 exhibited lower absorption coefficient than a-SiO$_x$:H(p). This can be attributed to the indirect bandgap property of $\mu$c-Si:H phase in $\mu$c-SiO$_x$:H(p) films. In addition, the absorption coefficient of $\mu$c-SiO$_x$:H(p) would depend on $X_C$. As $R_{H_2}$ increased from 175 to 300, the increased crystalline phase resulted in the decreased absorption coefficient.

Figure 4 shows the dependence of $R_{H_2}$ on dark conductivity ($\sigma_d$) and activation energy ($E_a$) of SiO$_x$:H(p). Our standard a-SiC$_x$:H(p) was also shown as a reference. Compared to a-SiO$_x$:H(p) with $R_{H_2}$ of 10, the a-SiC$_x$:H(p) deposited at the same $R_{H_2}$ exhibited lower $\sigma_d$ of $2.37 \times 10^{-7}$ S/cm and higher $E_a$ of 0.62 eV. Similar results were found by Fujikake et al. [27]. This improvement in $\sigma_d$ and $E_a$ of a-SiO$_x$:H(p) was ascribed to the higher mobility and the lower defect density than a-SiC$_x$:H(p) [27]. In the case of SiO$_x$:H(p), with increasing $R_{H_2}$ from 10 to 167, $\sigma_d$ was increased from $4.44 \times 10^{-7}$ to $1.15 \times 10^{-5}$ S/cm. This was because the increase in hydrogen radicals assisted etching the disorder configurations, providing energy for structural relaxation and passivating the dangling bonds in network, leading to reduced defect density and enhanced $\sigma_d$ [25]. Further increasing $R_{H_2}$ from 167 to 300, $\sigma_d$ was significantly increased from $1.15 \times 10^{-5}$ S/cm to $2.01 \times 10^{-1}$ S/cm. This could be due to the formation of crystalline structure as illustrated in Figure 1. The increased $\mu$c-Si:H phase and the enhanced $X_C$ could assist the carrier transport in film, thus increasing $\sigma_d$ of $\mu$c-SiO$_x$:H(p). In addition, with increasing $R_{H_2}$ from 10 to 300, $E_a$ was substantially decreased from 0.61 to 0.07 eV. This was due to the fact that the doping efficiency was higher in crystalline phase than that in amorphous phase [28]. In consequence, $R_{H_2}$ should be carefully controlled to prepare SiO$_x$:H(p) possessing the appropriate optoelectrical properties that are suitable for the cell application.

*3.2. Application of p-Type SiO$_x$:H as Window Layer in a-Si:H Single-Junction Cells.* The performance of a-Si:H single-junction solar cells employing SiO$_x$:H(p) deposited at different $R_{H_2}$ is demonstrated in Figure 5. As shown in Figure 5(a), with increasing $R_{H_2}$ from 10 to 167, the open-circuit voltage ($V_{OC}$) was increased from 0.89 to 0.91 V, which was due to the increased $E_g$ of SiO$_x$:H(p) from 1.96 to 2.04 eV. Further increasing $R_{H_2}$ from 167 to 300, $V_{OC}$ was decreased from 0.91

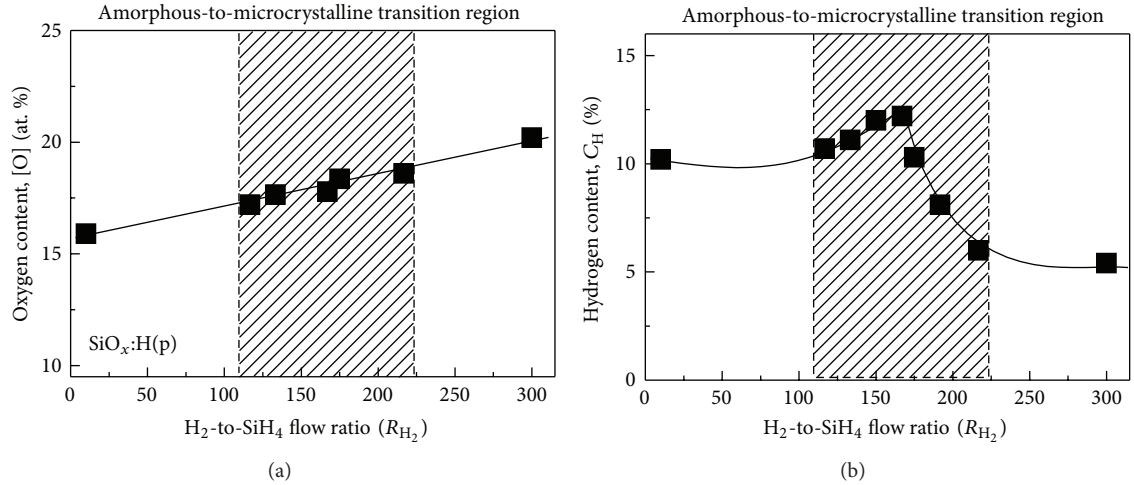


FIGURE 2: Effect of $R_{H_2}$ on (a) oxygen content and (b) hydrogen content of SiO$_x$:H(p) films.

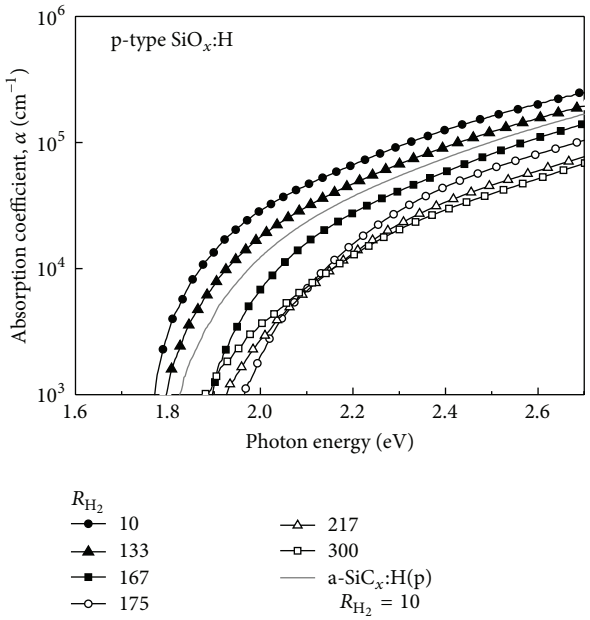


FIGURE 3: Effect of $R_{H_2}$ on absorption coefficient of SiO$_x$:H(p) films.

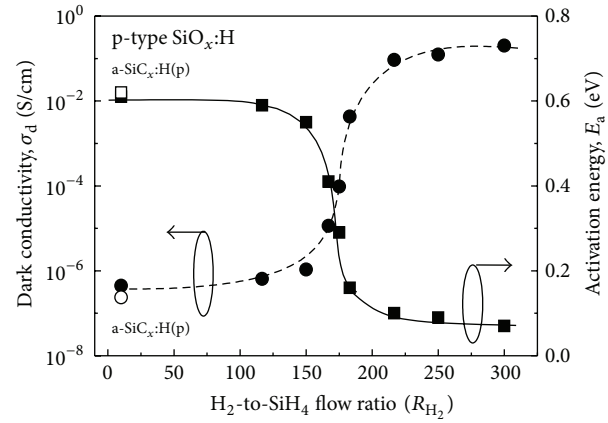


FIGURE 4: Effect of $R_{H_2}$ on dark conductivity and activation energy of SiO$_x$:H(p) films.

to 0.83 V. The decreased $V_{OC}$ can be ascribed to the structural defects at the p/i interface because of the interfacial lattice mismatch between $\mu$c-SiO$_x$:H(p) and a-Si:H(i). This led to the increased shunt leakage current and thus decreased $V_{OC}$ [29].

The effect of $R_{H_2}$ of SiO$_x$:H(p) on external quantum efficiency (EQE) of a-Si:H single-junction solar cells is illustrated in Figure 6. As $R_{H_2}$ was increased from 10 to 167, the EQE of short-wavelength region was enhanced gradually, which led to the increase in short-circuit current ($J_{SC}$) from 13.0 to 13.7 mA/cm$^2$ as shown in Figure 5(b). This was due to the reduced parasitic absorption loss arising from the increased $E_g$ of a-SiO$_x$:H(p). As $R_{H_2}$ was further increased from 167 to 300, the continuously enhanced EQE in short-wavelength region was observed, which was attributed to the reduction of optical loss by using $\mu$c-SiO$_x$:H(p). However, the slight reduction in EQE of long-wavelength region from 600 to 750 nm suggested that the defects presented at p/i interface hindered the carrier transport, which resulted from the heterogeneous nature between microcrystalline SiO$_x$:H p-layer and amorphous silicon absorber. $J_{SC}$ was thus decreased from 13.7 to 13.3 mA/cm$^2$ with increasing $R_{H_2}$ from 167 to 300.

The dependence of series resistance ($R_s$) and shunt resistance ($R_{sh}$) of a-Si:H cells on $R_{H_2}$ of SiO$_x$:H(p) layer is illustrated in Figure 7. With increasing $R_{H_2}$ from 10 to 167, $R_s$ was significantly decreased from 11.7 to 5.2 ohm·cm$^2$. This was due to the enhanced $\sigma_d$ of a-SiO$_x$:H(p) resulting from the reduced defect density. This could support the notion that the increased $C_H$ of a-SiO$_x$:H(p) (Figure 2(b)) was due to improved passivation of dangling bonds by hydrogen atoms. The quality of p/i interface was improved, leading to an increment in $R_{sh}$ from 1005 to 1739 ohm·cm$^2$. Therefore, with increasing $R_{H_2}$ from 10 to 167, the decreased $R_s$ and the increased $R_{sh}$ could enhance the FF from 65 to 70%, as shown in Figure 5(c). As $R_{H_2}$ further increased from 167 to 300, $R_s$

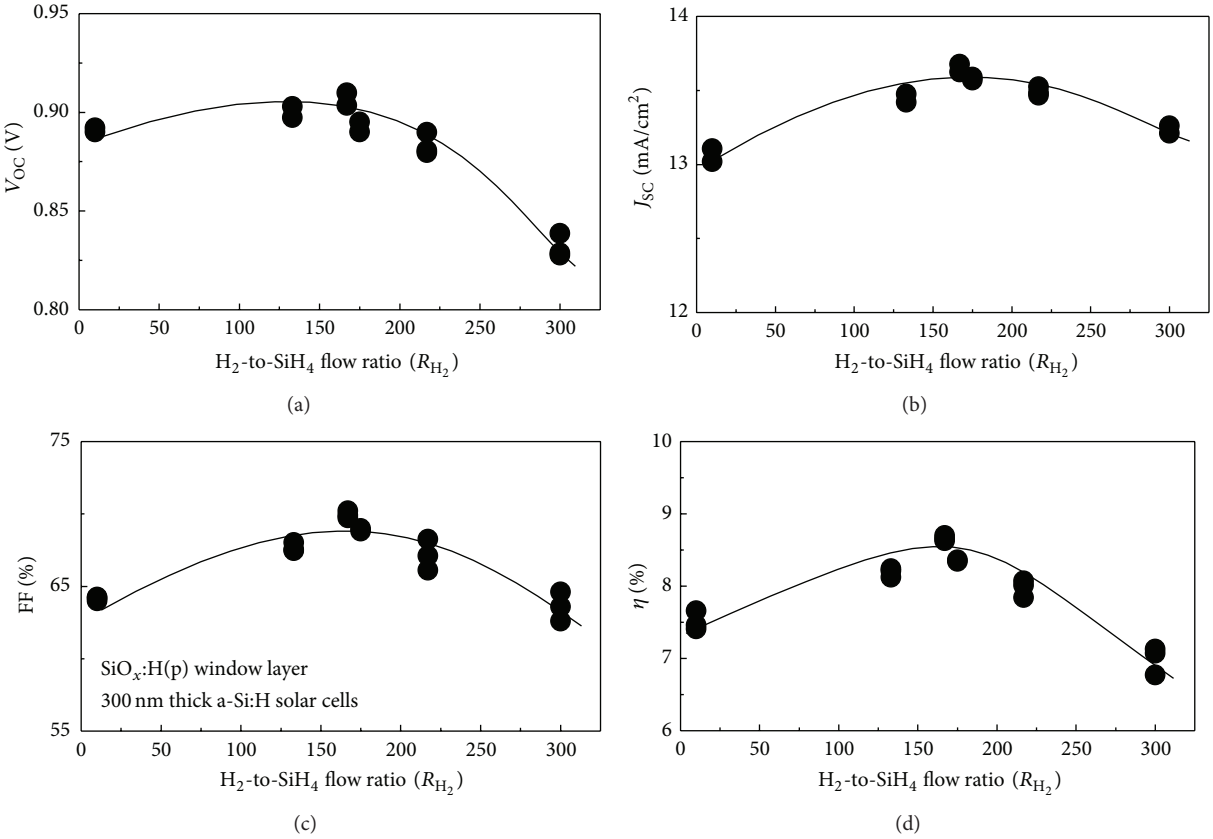


Figure 5: Performance of a-Si:H single-junction solar cells with $SiO_x$:H(p) of different $R_{H_2}$.

was decreased from 5.2 to 4.5 ohm·cm$^2$, which was likely due to the increased $\sigma_d$ resulting from the increased $X_C$ of $\mu$c-$SiO_x$:H(p). However, as $R_{H_2}$ was increased from 167 to 300, $R_{sh}$ was decreased from 1739 to 1160 ohm·cm$^2$. This was due to the interfacial lattice mismatch between $\mu$c-$SiO_x$:H(p) and a-Si:H(i) where defects were induced and thus increased the shunt leakage current. The decreased $R_{sh}$ counterbalanced the increased $R_s$ in this case, leading to a reduction of FF from 70 to 64%. As a result, the optimal a-Si:H cell performance that employed $SiO_x$:H(p) deposited at $R_{H_2}$ of 167 as window layer exhibited an efficiency of 8.7%, with $V_{OC}$ of 0.91 V, $J_{SC}$ of 13.7 mA/cm$^2$, and FF of 70%.

*3.3. Comparison of $SiO_x$:H(p) and a-$SiC_x$:H(p) as Window Layers in a-Si:H/a-$Si_{1-y}Ge_y$:H Tandem Cells.* Figure 8 illustrated the spectral response of a-Si:H/a-$Si_{1-y}Ge_y$:H tandem cells with $SiO_x$:H(p) and a-$SiC_x$:H(p) as window layers. The $SiO_x$:H(p) was prepared using $R_{H_2}$ of 167 while the a-$SiC_x$:H(p) was deposited using our standard condition. It can be seen that the employment of $SiO_x$:H(p) had a significant enhancement in EQE of short-wavelength range compared to that of a-$SiC_x$:H(p). The increment in short-wavelength range was due to the lower absorption coefficient of $SiO_x$:H(p) than that of a-$SiC_x$:H(p), leading to reduced parasitic absorption loss in window layer and increased $J_{SC}$ of top cell from 9.10 to 9.33 mA/cm$^2$.

The cell performance of a-Si:H/a-$Si_{1-y}Ge_y$:H tandem solar cells employing a-$SiC_x$:H(p) and $SiO_x$:H(p) layers is summarized in Table 1. Compared to standard a-$SiC_x$:H(p), the cell employing $SiO_x$:H(p) as window layer exhibited increased FF from 64.2 to 68.9%. As aforementioned, the increased $C_H$ of $SiO_x$:H(p) was related to the improved passivation of dangling bonds, resulting in less defects at the interface. In addition, the conductivity of $SiO_x$:H(p) was higher than that of a-$SiC_x$:H(p), which may reduce the electrical loss across the p-type layer. These two factors resulted in improved FF. Consequently, the a-Si:H/a-$Si_{1-y}Ge_y$:H tandem solar cell with the current matching optimization employing the $SiO_x$:H(p) deposited at $R_{H_2}$ of 167 as window layer exhibited a high efficiency of 10.3%, $V_{OC}$ of 1.60 V, $J_{SC}$ of 9.33 mA/cm$^2$, and FF of 68.9%. There was a relative efficiency enhancement of 11% compared to a-$SiC_x$:H(p) as window layer.

## 4. Conclusion

In this work, the effect of $R_{H_2}$ on structural, optical, and electrical properties of $SiO_x$:H(p) films in the amorphous-to-microcrystalline transition region was studied systematically. The $SiO_x$:H(p) films prepared by increasing $R_{H_2}$ from 10 to 167 increased $C_H$ due to the enhanced passivation of dangling bonds, resulting in the less defects in $SiO_x$:H(p). In addition, with increasing $R_{H_2}$ from 10 to 167, the increased bandgap and the increased conductivity of $SiO_x$:H(p) coincided with the increased $C_H$ by the improved passivation. Further increase of $R_{H_2}$ from 167 to 300 led to crystallite formation which increased the conductivity and $X_C$.

Table 1: Performance of a-Si:H/a-$Si_{1-y}Ge_y$:H tandem cells with different window layers.

| Window layer | $V_{OC}$ (V) | $J_{SC,top}$ (mA/cm$^2$) | $J_{SC,bot.}$ (mA/cm$^2$) | $J_{SC,total}$ (mA/cm$^2$) | FF (%) | $\eta$ (%) |
|---|---|---|---|---|---|---|
| $SiO_x$:H(p) | 1.60 | 9.33 | 9.36 | 18.69 | 68.9 | 10.3 |
| a-$SiC_x$:H(p) | 1.60 | 9.10 | 9.25 | 18.35 | 64.2 | 9.3 |

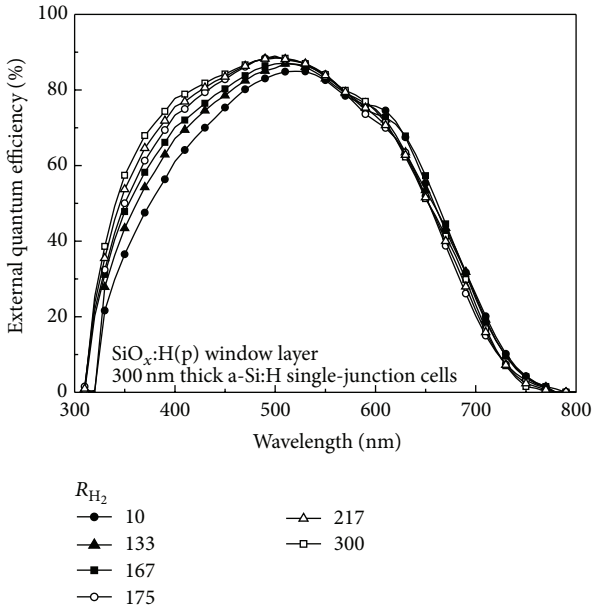


Figure 6: Spectral response of a-Si:H single-junction solar cells with $SiO_x$:H(p) of different $R_{H_2}$.

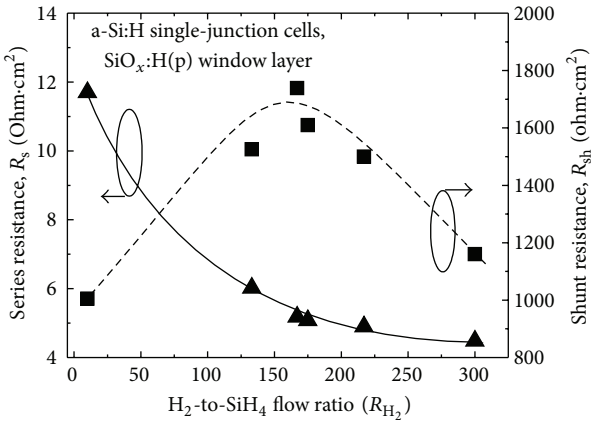


Figure 7: Effect of $R_{H_2}$ on series resistance and shunt resistance of a-Si:H single-junction solar cells.

By employing $SiO_x$:H(p) prepared by increasing $R_{H_2}$ from 10 to 300 in a-Si:H single-junction cells as the window layer, the short-wavelength spectral response was enhanced significantly. This was due to the reduced absorption coefficient of p-layers. However, as $R_{H_2}$ of $SiO_x$:H(p) was over 167, the defects at p/i interface hindered the carrier transport, which resulted from the heterogeneous nature between microcrystalline $SiO_x$:H p-layer and amorphous silicon absorber. The high FF of 70% and the efficiency of 8.7% were obtained

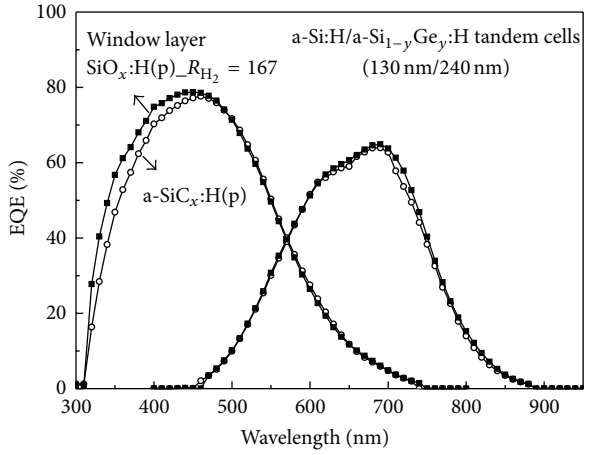


Figure 8: Spectral response of a-Si:H/a-$Si_{1-y}Ge_y$:H tandem cells with different window layers.

by employing $SiO_x$:H(p) deposited at $R_{H_2}$ of 167, which was attributed to the better film quality and the improved p/i interface. In the case of a-Si:H/a-$Si_{1-y}Ge_y$:H tandem cells designed for triple-junction solar cells, the replacement of standard a-$SiC_x$:H(p) by $SiO_x$:H(p) as window layer improved the efficiency from 9.3% to 10.3%, which was a relative enhancement of 11%.

## Competing Interests

The authors do not have any competing interests concerning the content of the paper.

## Acknowledgments

This work was sponsored by the Ministry of Science and Technology in Taiwan under Grant no. 103-3113-P-008-001. Besides, the authors gratefully thank Hung-Jung Hsu and Cheng-Hang Hsu for the continuous support and encouragement.

## References

[1] K. L. Chopra, P. D. Paulson, and V. Dutta, "Thin-film solar cells: an overview," *Progress in Photovoltaics: Research and Applications*, vol. 12, no. 2-3, pp. 69–92, 2004.

[2] A. V. Shah, H. Schade, M. Vanecek et al., "Thin-film silicon solar cell technology," *Progress in Photovoltaics: Research and Applications*, vol. 12, no. 2-3, pp. 113–142, 2004.

[3] M. A. Green, "Third generation photovoltaics: ultra-high conversion efficiency at low cost," *Progress in Photovoltaics: Research and Applications*, vol. 9, no. 2, pp. 123–135, 2001.

[4] O. Isabella, A. H. M. Smets, and M. Zeman, "Thin-film silicon-based quadruple junction solar cells approaching 20% conversion efficiency," *Solar Energy Materials and Solar Cells*, vol. 129, pp. 82–89, 2014.

[5] M. Stutzmann, R. A. Street, C. C. Tsai, J. B. Boyce, and S. E. Ready, "Structural, optical, and spin properties of hydrogenated amorphous silicon–germanium alloys," *Journal of Applied Physics*, vol. 66, no. 2, pp. 569–592, 1989.

[6] E. Maruyama, S. Okamoto, A. Terakawa, W. Shinohara, M. Tanaka, and S. Kiyama, "Toward stabilized 10% efficiency of large-area ($>5000\,cm^2$) a-Si/a-SiGe tandem solar cells using high-rate deposition," *Solar Energy Materials and Solar Cells*, vol. 74, no. 1–4, pp. 339–349, 2002.

[7] S. Okamoto, E. Maruyama, A. Terakawa et al., "Towards large-area, high-efficiency a-Si/a-SiGe tandem solar cells," *Solar Energy Materials and Solar Cells*, vol. 66, no. 1–4, pp. 85–94, 2001.

[8] A. Banerjee, "Study of top contact/p-layer junction for the optimization of large-area amorphous silicon multijunction cells," *Solar Energy Materials and Solar Cells*, vol. 36, no. 3, pp. 295–299, 1995.

[9] R. Biron, C. Pahud, F.-J. Haug, J. Escarré, K. Söderström, and C. Ballif, "Window layer with p doped silicon oxide for high $V_{OC}$ thin-film silicon n-i-p solar cells," *Journal of Applied Physics*, vol. 110, no. 12, Article ID 124511, 2011.

[10] Y. Hattori, D. Kruangam, T. Toyama, H. Okamoto, and Y. Hamakawa, "Valency control of P-type a-SiC: H having the optical band gap more than 2.5 eV by electron-cyclotron resonance CVD (ECR CVD)," *Journal of Non-Crystalline Solids*, vol. 1079, pp. 97–98, 1987.

[11] A. Sarker and A. K. Barua, "Development of high quality p-type hydrogenated amorphous silicon oxide film and its use in improving the performance of single junction amorphous silicon solar cells," *Japanese Journal of Applied Physics, Part 1: Regular Papers and Short Notes and Review Papers*, vol. 41, no. 2, pp. 765–769, 2002.

[12] S. Inthisang, T. Krajangsang, I. A. Yunaz, A. Yamada, M. Konagai, and C. R. Wronski, "Fabrication of high open-circuit voltage a-$Si_{1-x}O_x$:H solar cells by using p-a-$Si_{1-x}O_x$:H as window layer," *Physica Status Solidi (C) Current Topics in Solid State Physics*, vol. 8, no. 10, pp. 2990–2993, 2011.

[13] S. Guha, J. Yang, A. Banerjee, B. Yan, and K. Lord, "High quality amorphous silicon materials and cells grown with hydrogen dilution," *Solar Energy Materials & Solar Cells*, vol. 78, no. 1–4, pp. 329–347, 2003.

[14] S. Guha, J. Yang, D. L. Williamson, Y. Lubianiker, J. D. Cohen, and A. H. Mahan, "Structural, defect, and device behavior of hydrogenated amorphous Si near and above the onset of microcrystallinity," *Applied Physics Letters*, vol. 74, no. 13, pp. 1860–1862, 1999.

[15] S. Inthisang, K. Sriprapha, S. Miyajima, A. Yamada, and M. Konagai, "Hydrogenated amorphous silicon oxide solar cells fabricated near the phase transition between amorphous and microcrystalline structures," *Japanese Journal of Applied Physics*, vol. 48, no. 12, Article ID 122402, 2009.

[16] C. R. Wronski and R. W. Collins, "Phase engineering of a-Si:H solar cells for optimized performance," *Solar Energy*, vol. 77, no. 6, pp. 877–885, 2004.

[17] J. Tauc, "Optical properties and electronic structure of amorphous Ge and Si," *Materials Research Bulletin*, vol. 3, no. 1, pp. 37–46, 1968.

[18] S. Y. Myong, K. Sriprapha, S. Miyajima, M. Konagai, and A. Yamada, "High efficiency protocrystalline silicon/microcrystalline silicon tandem cell with zinc oxide intermediate layer," *Applied Physics Letters*, vol. 90, no. 26, Article ID 263509, 2007.

[19] Y. Hishikawa, "Raman study on the variation of the silicon network of a-Si:H," *Journal of Applied Physics*, vol. 62, no. 8, pp. 3150–3155, 1987.

[20] R. L. C. Vink, G. T. Barkema, and W. F. van der Weg, "Raman spectra and structure of amorphous Si," *Physical Review B*, vol. 63, no. 11, Article ID 115210, 2001.

[21] J. Y. Ahn, K. H. Jun, K. S. Lim, and M. Konagai, "Stable protocrystalline silicon and unstable microcrystalline silicon at the onset of a microcrystalline regime," *Applied Physics Letters*, vol. 82, no. 11, pp. 1718–1720, 2003.

[22] A. Asano, "Effects of hydrogen atoms on the network structure of hydrogenated amorphous and microcrystalline silicon thin films," *Applied Physics Letters*, vol. 56, no. 6, pp. 533–535, 1990.

[23] S. M. Iftiquar, "The roles of deposition pressure and rf power in opto-electronic properties of a-$SiO_x$:H films," *Journal of Physics D: Applied Physics*, vol. 31, no. 14, pp. 1630–1641, 1998.

[24] G. Lucovsky, J. Yang, S. S. Chao, J. E. Tyler, and W. Czubatyj, "Oxygen-bonding environments in glow-discharge-deposited amorphous silicon-hydrogen alloy films," *Physical Review B*, vol. 28, no. 6, pp. 3225–3233, 1983.

[25] C. C. Tsai, G. B. Anderson, R. Thompson, and B. Wacker, "Control of silicon network structure in plasma deposition," *Journal of Non-Crystalline Solids*, vol. 114, no. 1, pp. 151–153, 1989.

[26] D. Das, S. M. Iftiquar, D. Das, and A. K. Barua, "Improvement in the optoelectronic properties of a-SiO:H films," *Journal of Materials Science*, vol. 34, no. 5, pp. 1051–1054, 1999.

[27] S. Fujikake, H. Ohta, A. Asano, Y. Ichikawa, and H. Sakai, "High quality a-SiO:H films and their application to a-Si solar cells," *Material Research Society Symposium Proceedings*, vol. 258, p. 875, 1992.

[28] K. Prasad, U. Kroll, F. Finger et al., "Highly conductive microcrystalline silicon layers for tunnel junctions in stacked amorphous silicon based solar cells," *Material Research Society Symposium Proceedings*, vol. 219, p. 469, 1991.

[29] C. B. Roxlo, B. Abeles, and T. Tiedje, "Evidence for lattice-mismatch—induced defects in amorphous semiconductor heterojunctions," *Physical Review Letters*, vol. 52, no. 22, pp. 1994–1997, 1984.